Cumulative inactivation of N-type $Ca_V2.2$ calcium channels modified by alternative splicing

Christopher Thaler*†, Annette C. Gray†‡, and Diane Lipscombe‡§

*Laboratory of Molecular Physiology, Section on Cellular Biophotonics, National Institute on Alcohol Abuse and Alcoholism, National Institutes of Health, Rockville, MD 20852; and ‡Department of Neuroscience, Brown University, Providence, RI 02912

Edited by Harald Reuter, University of Bern, Bern, Switzerland, and approved February 17, 2004 (received for review June 5, 2003)

The Ca_V2 family of voltage-gated calcium channels, present in presynaptic nerve terminals, regulates exocytosis and synaptic transmission. Cumulative inactivation of these channels occurs during trains of action potentials, and this may control short-term dynamics at the synapse. Inactivation during brief, repetitive stimulation is primarily attributed to closed-state inactivation, and several factors modulate the susceptibility of voltage-gated calcium channels to this form of inactivation. We show that alternative splicing of an exon in a cytoplasmic region of the $Ca_V2.2$ channel modulates its sensitivity to inactivation during trains of action potential waveforms. The presence of this exon, exon 18a, protects the $Ca_V2.2$ channel from entry into closed-state inactivation specifically during short (10 ms to 3 s) and small depolarizations of the membrane potential (−60 mV to −50 mV). The reduced sensitivity to closed-state inactivation within this dynamic range likely underlies the differential responsiveness of $Ca_V2.2$ splice isoforms to trains of action potential waveforms. Regulated alternative splicing of $Ca_V2.2$ represents a possible mechanism for modulating short-term dynamics of synaptic efficacy in different regions of the nervous system.

The Ca_V2 class of voltage-gated calcium channels regulates calcium entry that triggers exocytosis from presynaptic nerve terminals (1). The temporal dynamics of calcium channel responses to action potential trains impact the fidelity of synaptic transmission (2). Membrane depolarization both activates and inactivates voltage-gated calcium channels. With repetitive, brief depolarizations, inactivation of calcium channels accumulates over time and progressively decreases calcium entry.

Cumulative inactivation, a feature of both native and cloned Ca_V2 calcium channels, has been studied in detail because of its importance in regulating the short-term dynamics of synaptic efficacy (2–8). Inactivation that accumulates during brief, repetitive stimulation is thought to result from a process known as closed-state inactivation (5, 6). That is, voltage-gated calcium channels undergo inactivation in response to depolarizations that are insufficiently large to open the channel. Open-state inactivation is thought to play only a minor role in cumulative inactivation of Ca_V2 calcium channels during brief stimuli such as action potentials. Even during prolonged depolarizations that favor open-state inactivation, Ca_V2 channels inactivate with relatively slow time courses. Only in the case of Ca_V3 channels that deactivate relatively slowly following action potential repolarization has open-state inactivation been implicated in cumulative inactivation (9–11). Several factors modulate the susceptibility of voltage-gated calcium channels to cumulative inactivation, including channel subtype (6), G protein activation (3), interaction with presynaptic proteins (12, 13), and alternative splicing (10, 11). However, a limited number of studies have investigated the mechanisms by which cumulative inactivation is modulated (12).

Voltage-gated calcium channels are subject to extensive alternative splicing, and in several cases this leads to changes in the time course and voltage dependence of channel inactivation (14). However, the effects of alternative splicing on the ability of Ca_V2 calcium channels to respond to more physiologically relevant stimuli, including action potential waveforms, has not been assessed. Furthermore, alternative splicing occurs most often in cytoplasmic regions of Ca_V2 channels (14), where effects on channel gating are hard to predict. In particular, exon 18a in the $Ca_V2.2$ genes of rat, mouse, and human encodes 21 aa in the cytoplasmic II–III loop. Its presence in $Ca_V2.2$ mRNAs is tissue-specific (15), possibly linked to monoaminergic neurons (16). Exon 18a modifies the voltage dependence of steady-state inactivation under certain conditions without affecting the kinetics or voltage dependence of channel activation (15). A homologous alternatively spliced exon whose expression is regulated is also present in the $Ca_V2.3$ gene (14, 17, 18). Functional studies of $Ca_V2.3$ channels that contain this exon indicate that it regulates the Ca sensitivity of certain channel properties (19, 20).

Here, we demonstrate that $Ca_V2.2$ splice isoforms that contain and lack exon 18a differ significantly in their susceptibility to inactivation during trains of action potential waveforms. The presence of exon 18a protects the channel from entry into closed-state inactivation, and this likely reduces cumulative inactivation. Regulated alternative splicing of $Ca_V2.2$ in the II–III loop may represent a mechanism for modulating short-term dynamics of synaptic efficacy.

Methods

Cell Culture. tsA-201 cells were grown in 89% DMEM, 10% FBS, and 1% penicillin/streptomycin. After plating, cells were transfected with plasmids containing $Ca_V2.2e[+18a]$ and $Ca_V2.2e[\Delta 18a]$ splice isoforms along with $Ca_V\beta_{1b}$, $Ca_V\alpha_2\delta_1$, and green fluorescent protein by using Lipofectamine-Plus or 2000 reagents (Invitrogen). $Ca_V2.2e[\Delta 18a]$ (AF055477) (21), $Ca_V2.2e[+18a]$ (AF222337) (15), and $Ca_V\alpha_2\delta_1$ (Y. Lin and D.L., unpublished data) (GenBank accession no. AF286488) were cloned in our laboratory. $Ca_V\beta_{1b}$ cDNA was provided by K.P. Campbell (University of Iowa, Iowa City; ref. 22). Recordings were performed 24–48 h after transfection.

Electrophysiology. Whole cell voltage-clamp recordings were performed by using an Axopatch 200 amplifier (Axon Instruments) in a bath consisting of 135 mM Choline Cl, 10 mM Hepes, 4 mM $MgCl_2$, and 1 mM $CaCl_2$, adjusted to a pH of 7.2 with TEA·OH or CsOH. The internal solution consisted of 135 mM CsCl, 10 mM Hepes, 1 mM EGTA, 1 mM EDTA, and 4 mM Mg-ATP, adjusted to a pH of 7.2 with TEA·OH or CsOH. PCLAMP 8 software was used for data acquisition (Axon Instruments). For square pulse protocols, data were filtered at 2 kHz and sampled at 20 kHz. For recordings using action potential waveforms as the command potential, data were filtered at 10 kHz and sampled at 100 kHz. Patch electrodes were 1–3 MΩ when filled with internal solution. Leak subtraction was performed online by using a P/−4 protocol. Series resistance compensation (70%)

This paper was submitted directly (Track II) to the PNAS office.

†C.T. and A.C.G. contributed equally to this work.

§To whom correspondence should be addressed. E-mail: diane_lipscombe@brown.edu.

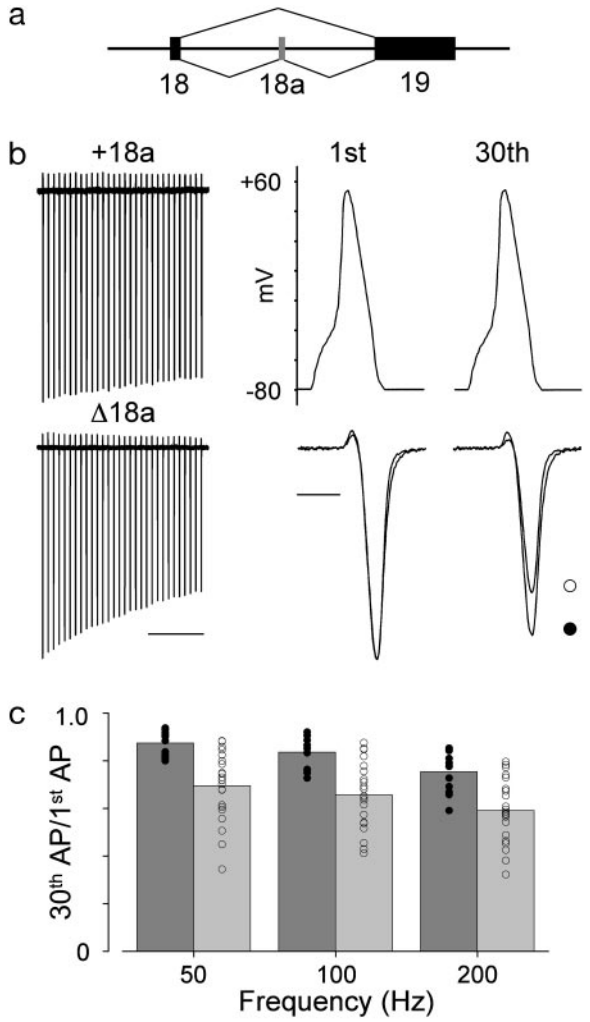

Fig. 1. $Ca_V2.2$ splice isoforms differ in their sensitivity to cumulative inactivation during action potential trains applied at 50, 100, and 200 Hz. (*a*) The structure of the $Ca_V2.2$ gene is shown for exons 18, 18a, and 19. The sequence can be found in the GenBank database (accession no. AF222338) (15). Exon 18a is located in the intracellular II–III loop region of $Ca_V2.2$, and its alternate expression generates $Ca_V2.2e[+18a]$ and $Ca_V2.2e[\Delta 18a]$ isoforms. (*b*) Comparison of currents generated by a train of action potential waveforms in tsA-201 cells expressing $Ca_V2.2e[+18a]$ and $Ca_V2.2e[\Delta 18a]$ together with $Ca_V\beta_{1b}$ and $Ca_V\alpha_2\delta_1$. Thirty action potential waveforms, with half-widths of 0.6 ms and peaks at +55 mV, were delivered at 50 Hz from a holding potential of −80 mV. First and 30th current traces from cells expressing $Ca_V2.2e[+18a]$ (●) and $Ca_V2.2e[\Delta 18a]$ (○) are shown, normalized to the peak current amplitude of the first action potential response. Action potential waveforms are displayed above the current traces. (*Left*: scale bar, 200 ms; *Right*: scale bar, 1 ms.) (*c*) Summary of cumulative inactivation of $Ca_V2.2e[+18a]$ and $Ca_V2.2e[\Delta 18a]$ isoforms after 50-, 100-, and 200-Hz trains. For these frequencies, $Ca_V2.2e[+18a]$ currents (dark gray) inactivated by 13 ± 1% (n = 12), 16 ± 2% (n = 12), and 25 ± 2% (n = 12), respectively. $Ca_V2.2e[\Delta 18a]$ currents (light gray) inactivated by 31 ± 3% (n = 22), 34 ± 3% (n = 22), and 41 ± 3% (n = 21), respectively. Individual data points for $Ca_V2.2e[+18a]$ (●) and $Ca_V2.2e[\Delta 18a]$ (○) are also shown. The difference between the isoforms was statistically significant at all frequencies tested ($P < 0.001$).

was used with a 10-μs lag. Statistical references indicate the mean ± SE. The presence of the $Ca_V2.2$ subunit was required to generate calcium channel currents in tsA-201 cells. Peak current densities were 190 ± 44 pA/pF and 224 ± 35 pA/pF in cells expressing $Ca_V2.2e[+18a]$ (n = 16) and $Ca_V2.2e[\Delta 18a]$ (n = 12) together with $Ca_V\beta_{1b}$ and $Ca_V\alpha_2\delta_1$. In contrast, no significant currents were recorded in cells transfected with $Ca_V\beta_{1b}$ and $Ca_V\alpha_2\delta_1$ alone (0.4 ± 0.4 pA/pF, n = 4).

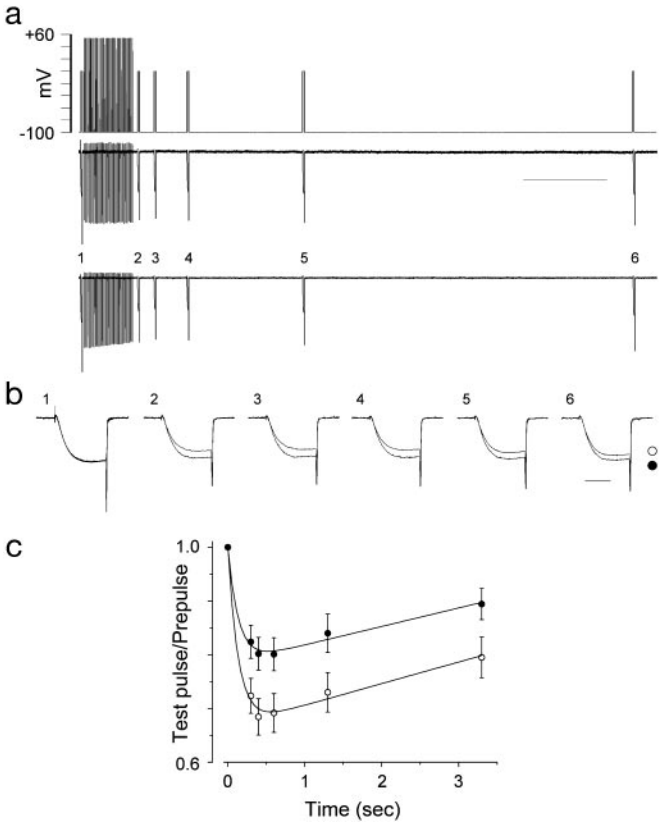

Fig. 2. Recovery from inactivation induced by action potential waveforms. (*a*) Cumulative inactivation of $Ca_V2.2$ currents was induced by 30 action potential waveforms applied at 100 Hz with a holding potential of −100 mV (*Top*). Representative current traces for the $Ca_V2.2e[+18a]$ (*Middle*) and $Ca_V2.2e[\Delta 18a]$ (*Bottom*). Test pulses to peak current were applied at various time intervals (2–6) after the train and compared to a test pulse before the train (1). (Scale bar, 500 ms.) (*b*) Currents are shown on an expanded time scale and normalized to peak current. (Scale bar, 5 ms.) (*c*) Values plotted are average, peak current amplitudes normalized to the amplitude of the pulse preceding the train, for $Ca_V2.2e[+18a]$ (●, n = 8) and $Ca_V2.2e[\Delta 18a]$ (○, n = 18). Before normalization, average peak current amplitudes of the pulse preceding the train were 3,686 ± 629 pA for $Ca_V2.2e[+18a]$ and 2,475 ± 289 pA for $Ca_V2.2e[\Delta 18a]$. These values are not significantly different ($P > 0.05$). Average peak current amplitudes for the first test pulse after the train were 2,863 ± 445 pA for $Ca_V2.2e[+18a]$ and 1,762 ± 216 pA for $Ca_V2.2e[\Delta 18a]$. Current amplitudes were significantly different between splice isoforms at the 100-ms time point ($P < 0.05$). The data were fit with an exponential linear function: $y = A_1[e^{(-x/\tau)}] + y_0 + A_2x$. Time constants and slopes that estimate the rate of recovery from inactivation were not significantly different between isoforms ($P > 0.6$).

Results

The intracellular II–III loop ($L_{II\text{-}III}$) of the $Ca_V2.2$ subunit is encoded by exons 18–21 in rat, mouse, and human genomes (15, 23, 24) (Fig. 1*a*). Exon 18a encodes 21 aa, and its inclusion in $Ca_V2.2$ mRNAs is regulated at the cellular level. Specifically, $Ca_V2.2$ mRNAs containing exon 18a are abundant in peripheral ganglia, spinal cord, and in caudal regions of the brain, but are less prevalent in adult neocortex, cerebellum, and hippocampus (15, 16). Alternative splicing in $L_{II\text{-}III}$ of $Ca_V2.2$ that involves exons 18a (15) or exons 19 through 21 (25) modifies channel inactivation properties without affecting the kinetics or voltage dependence of channel activation. However, it is not known whether alternative splicing in $Ca_V2.2$ influences the ability of the channel to respond to more physiologically relevant stimuli, such as a train of action potentials.

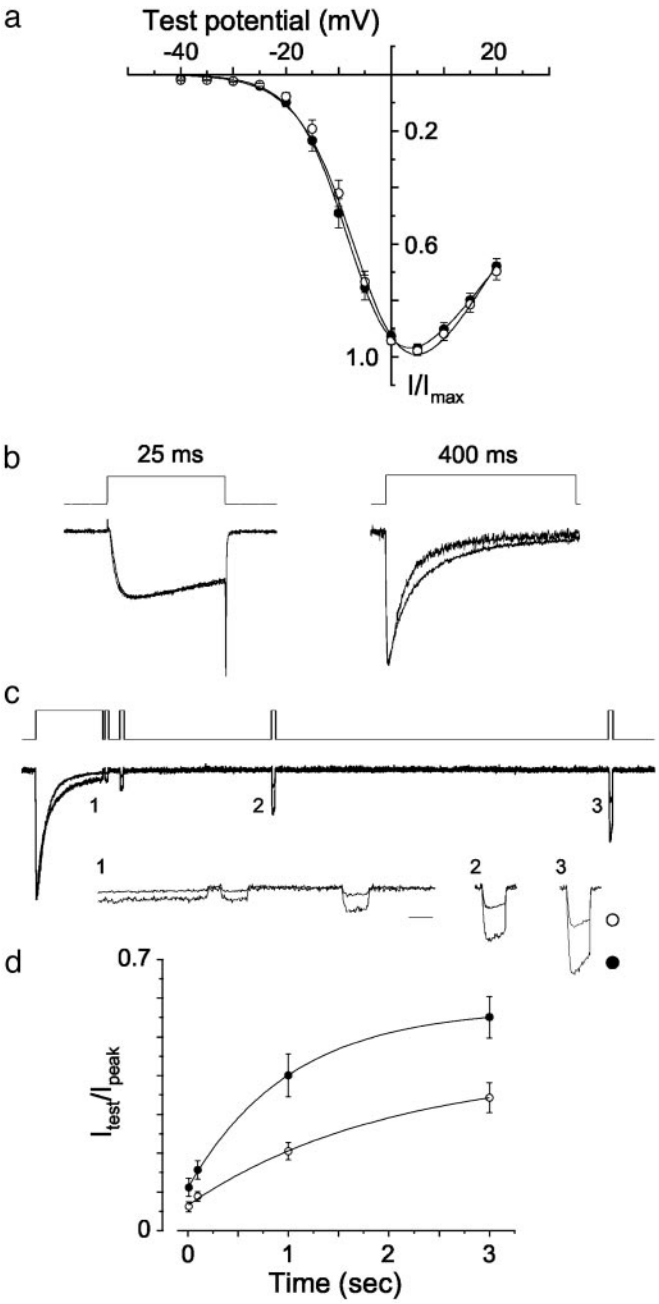

Fig. 3. Properties of splice isoforms studied with pulse protocols that activate the channel. (*a*) Averaged, normalized N-type current–voltage relationships were measured from cells expressing $Ca_V2.2e[+18a]$ (●, $n = 16$) and $Ca_V2.2e[\Delta 18a]$ (○, $n = 12$) from a holding potential of −100 mV. (*b*) Currents generated by 25-ms and 400-ms square-pulse depolarizations to peak current. The average decrease in current at the end of the 25-ms depolarization was 23 ± 3% ($n = 16$) for $Ca_V2.2e[+18a]$ compared with 25 ± 5% ($n = 10$) for $Ca_V2.2e[\Delta 18a]$. These values are not significantly different ($P > 0.6$). Average decay time constants for $Ca_V2.2$ currents induced by 400-ms step depolarizations were obtained from exponential fits to the inactivation phase. Time constants were 62 ± 8 ms ($n = 6$) and 49 ± 4 ms ($n = 9$) for $Ca_V2.2e[+18a]$ and $Ca_V2.2e[\Delta 18a]$, respectively ($P = 0.1$). (*c*) A 400-ms test pulse to 0 mV was applied to induce open-state inactivation, followed by shorter test pulses (20 ms) to assess the degree and rate of recovery. The voltage protocol (*Top*) and sample current traces (*Middle*) are shown. Sections of the current traces (1–3) are expanded (*Bottom*; scale bar, 20 ms). (*d*) Time course of recovery from inactivation for $Ca_V2.2e[+18a]$ (●, $n = 11$) and $Ca_V2.2e[\Delta 18a]$ (○, $n = 12$) currents. Values shown are averaged and normalized to the peak current amplitude of the 400-ms test pulse. At the 10-ms time point, $Ca_V2.2e[+18a]$ channels were 11 ± 2% of the peak current compared with 6 ± 1% for $Ca_V2.2e[\Delta 18a]$ ($P = 0.08$). At 100 ms, $Ca_V2.2e[+18a]$ channels had recovered to 16 ± 2% of the peak current value, whereas $Ca_V2.2e[\Delta 18a]$ channels recovered only slightly to 9 ± 1%. Values at 100 ms were significantly different ($P = 0.01$). The extent of recovery between isoforms at 1-s ($P < 0.003$) and 3-s ($P < 0.004$) time points were significantly different. Data were fit by using the equation $y = A[1 - e^{(-x/\tau)}] + y_0$. Time constants that estimate the rate of recovery from inactivation were not significantly different between isoforms ($P = 0.62$).

Cumulative Inactivation During Trains of Action Potential Waveforms. We compared the responsiveness of $Ca_V2.2e[+18a]$ and $Ca_V2.2e[\Delta 18a]$ splice isoforms to a train of action potential waveforms and found that they differed significantly. $Ca_V2.2e[+18a]$ and $Ca_V2.2e[\Delta 18a]$ channels progressively inactivated during a train of 30 action potential waveforms delivered at 50 Hz (Fig. 1*b*). $Ca_V2.2e[+18a]$ currents inactivated by only 13 ± 1% ($n = 12$) by the end of the train, whereas $Ca_V2.2e[\Delta 18a]$ currents were reduced 31 ± 2% ($n = 22$), a >2-fold difference (Fig. 1 *b* and *c*, $P < 0.001$). The difference between splice isoforms was observed with trains at 50, 100, and 200 Hz and notably was independent of frequency (Fig. 1*c*, $P < 0.001$). This finding suggests that the interstimulus interval does not contribute to the difference between splice isoforms.

We also compared the time courses of recovery of $Ca_V2.2e[+18a]$ and $Ca_V2.2e[\Delta 18a]$ splice isoforms from cumulative inactivation induced by a train of action potential waveforms (Fig. 2). Brief test pulses applied at various time points after the train were compared to a prepulse given before the train. Although the extents of inactivation differed between isoforms (Fig. 1), the rates of recovery from cumulative inactivation were indistinguishable (Fig. 2*c*, $P > 0.6$). This, along with the frequency independence, suggests that alternative splicing modifies entry into, but not recovery from, inactivation. To investigate the mechanism underlying entry into inactivation, we used a variety of square-wave pulse protocols and assessed channel properties.

Basic Channel Properties. Current–voltage relationships of $Ca_V2.2e[+18a]$ and $Ca_V2.2e[\Delta 18a]$ channels were indistinguishable (Fig. 3*a*), consistent with our previous studies in *Xenopus* oocytes (15). Activation and inactivation kinetics of splice isoforms were also similar when studied with relatively short 25-ms square-wave depolarizing steps to activate and subsequently inactivate them (Fig. 3*b*, at the end of the pulse $Ca_V2.2e[+18a]$ inactivated by 23 ± 3%, $n = 16$, compared to 25 ± 5%, $n = 10$, for $Ca_V2.2e[\Delta 18a]$; $P > 0.6$). With longer 400-ms depolarizations, $Ca_V2.2e[+18a]$ channels tended to inactivate with a somewhat slower time course compared to $Ca_V2.2e[\Delta 18a]$ (Fig. 3*b*; $Ca_V2.2e[+18a]$ $\tau = 62 \pm 8$ ms, $n = 6$; $Ca_V2.2e[\Delta 18a]$ $\tau = 49 \pm 4$ ms, $n = 9$; $P = 0.1$).

Recovery from Open-State Inactivation. We compared the degree of recovery from open-state inactivation induced by a 400-ms depolarization for $Ca_V2.2e[+18a]$ and $Ca_V2.2e[\Delta 18a]$ channels (Fig. 3 *c* and *d*). Recovery was assessed with brief test pulses normalized to the peak of the initial depolarization. Whereas the extents of recovery differed between isoforms, the rates of recovery from inactivation were indistinguishable (Fig. 3 *c* and *d*, $P > 0.6$). However, the overall rate of entry into open-state inactivation was very slow compared to the rapid time course of an action potential.

Closed-State Inactivation. Next, we studied the voltage dependence of closed-state inactivation with small depolarizations that do not open the channel. We applied relatively long 30-s prepulses at different holding potentials to assess channel availability under steady-state conditions. When this paradigm was

PHYSIOLOGY

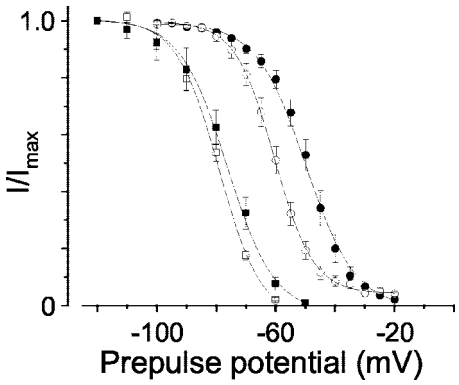

Fig. 4. The voltage dependence of closed-state inactivation. Averaged, normalized, steady-state inactivation curves were generated from cells expressing $Ca_V2.2e[+18a]$ (■, $n = 3$) and $Ca_V2.2e[\Delta 18a]$ (□, $n = 3$). Thirty-second prepulses to the indicated holding potentials were followed by a 50-ms test pulse to measure channel availability. Averaged $V_{1/2}$ values were -78 ± 2 mV for $Ca_V2.2e[+18a]$ and -78 ± 0.8 mV for $Ca_V2.2e[\Delta 18a]$. These values were not significantly different. Inactivating channels with 3-s prepulses to the indicated holding potentials revealed significant differences between isoforms. $V_{1/2}$ values were -48 ± 3 mV for $Ca_V2.2e[+18a]$ (●, $n = 8$) and -60 ± 4 mV for $Ca_V2.2e[\Delta 18a]$ (○, $n = 8$; $P < 0.0001$).

used, $Ca_V2.2e[+18a]$ and $Ca_V2.2e[\Delta 18a]$ channels inactivated with the same voltage dependence (Fig. 4, $P > 0.05$). Long prepulses, however, do not necessarily indicate how channels will respond to brief membrane depolarizations such as trains of action potentials. We therefore applied shorter prepulses to induce closed-state inactivation. Predictably, under these conditions, more depolarized membrane voltages were required to induce channel inactivation. Most importantly, however, this short prepulse paradigm revealed a significant difference in the voltage dependence of closed-state inactivation between splice isoforms. $Ca_V2.2e[+18a]$ channels inactivated at voltages ≈10 mV more depolarized than $Ca_V2.2e[\Delta 18a]$ (Fig. 4, $P < 0.0001$).

Closed-State Inactivation at Early Time Points. We next explored the possibility that differences in closed-state inactivation between $Ca_V2.2e[+18a]$ and $Ca_V2.2e[\Delta 18a]$ splice isoforms might be apparent at even earlier time points after small membrane depolarizations. Indeed, the degree of closed-state inactivation immediately following a stimulus is likely to be highly relevant to inactivation that accumulates during action potential trains. We used protocols (6) to induce closed-state inactivation at early time points (Fig. 5). When the membrane potential during the interpulse interval was set at −80 mV, we found no significant difference in the sensitivity of $Ca_V2.2e[+18a]$ and $Ca_V2.2e[\Delta 18a]$ channels to entry into closed-state inactivation. However, when splice isoforms were compared by using a moderately more depolarized interpulse holding potential of −60 mV, $Ca_V2.2e[+18a]$ channels resisted entry into closed-state inactivation as compared to $Ca_V2.2e[\Delta 18a]$. This is consistent with the difference in the voltage dependence of closed-state inactivation between $Ca_V2.2$ isoforms assessed with relatively short prepulses (Fig. 4). At a membrane potential of −80 mV, both isoforms are fully available for activation, whereas at −60 mV a significantly greater fraction of $Ca_V2.2e[+18a]$ channels is available (Fig. 4, $P < 0.0001$).

Our data have shown that $Ca_V2.2$ splice isoforms differ significantly with respect to their entry into closed-state inactivation induced by brief depolarizations. The greater sensitivity of $Ca_V2.2e[\Delta 18a]$ channels to cumulative inactivation during trains of action potential waveforms is therefore best explained by a greater sensitivity to entry into closed-state inactivation compared to $Ca_V2.2e[+18a]$.

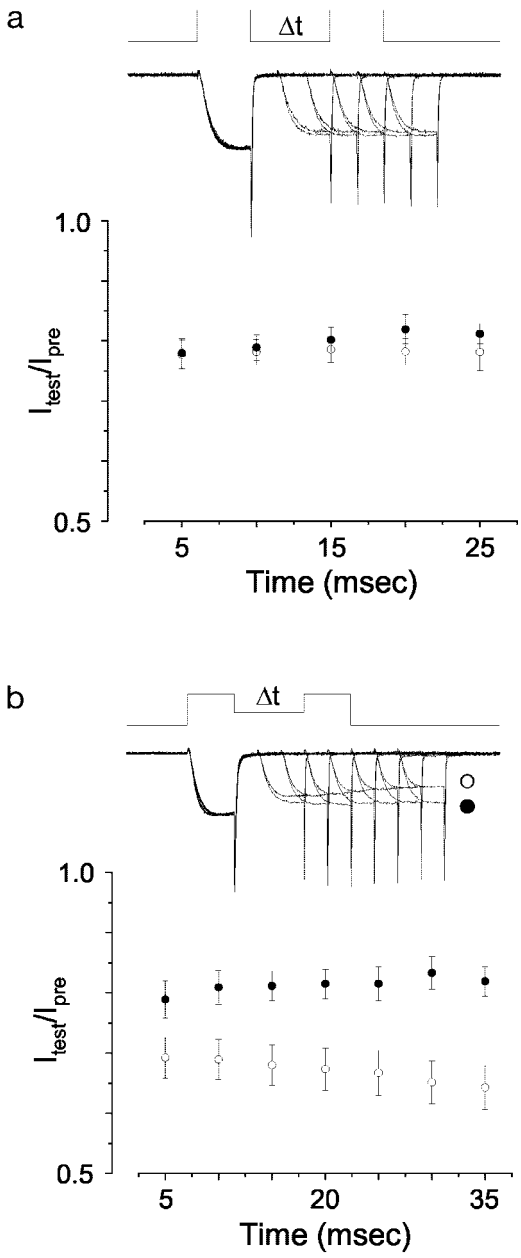

Fig. 5. Entry into closed-state inactivation. Voltage protocols and sample current traces are shown in *a Upper* and *b Upper*. (*a*) A double-pulse preferential closed-state inactivation protocol (6, 7) was used to compare the sensitivity of $Ca_V2.2e[+18a]$ (●, $n = 9$) and $Ca_V2.2e[\Delta 18a]$ (○, $n = 8$) channels to closed-state inactivation (holding potential = −80 mV). Values plotted are average, normalized peak currents. There was no significant difference in the amount of closed-state inactivation (20–25%) between splice isoforms at all time points tested ($P > 0.05$). (*b*) By using a similar double-pulse protocol with a more depolarized holding potential (−60 mV) between pulses, significant differences in entry into closed-state inactivation were observed between $Ca_V2.2e[+18a]$ (●, $n = 8$) and $Ca_V2.2e[\Delta 18a]$ (○, $n = 10$) ($P < 0.05$ at all points except 5 ms).

Discussion

In this study, we demonstrate that the inclusion of exon 18a in the intracellular II–III loop of the $Ca_V2.2$ subunit modifies the dynamic properties of the channel in response to trains of action potential waveforms. Exon 18a decreases the degree of cumulative inactivation of the channel by protecting it from entry into closed-state inactivation. Differences in closed-state inactivation

between isoforms were observed following small, brief membrane depolarizations that were within the temporal range relevant to action potential trains (Figs. 1, 4, and 5). Furthermore, splice isoforms differed in their degree of cumulative inactivation independent of stimulus frequency. This supports a mechanism involving entry into, but not recovery from, closed-state inactivation. We observed a small difference in the rate of entry into open-state inactivation between isoforms that may also contribute. However, this difference was only evident with prolonged 400-ms depolarizations, significantly longer than the total time spent in the open state during an action potential train.

Different classes of neuronal calcium channels vary in their susceptibility to cumulative inactivation (6, 11). Closed-state inactivation is the mechanism thought to underlie cumulative inactivation of high-voltage-activated neuronal channels when induced by trains of action potential waveforms (5, 6). Our results are consistent with these studies. In addition, we demonstrate that alternative splicing can regulate this process. Our results are also consistent with previous recordings in *Xenopus* oocytes where we observed an ≈10-mV difference in the voltage dependence of inactivation between $Ca_V2.2e[+18a]$ and $Ca_V2.2e[\Delta 18a]$ splice isoforms when expressed with $Ca_V\beta_{1b}$ (15).

The mechanism by which the inclusion of exon 18a in the II–III loop of $Ca_V2.2$ protects the channel from closed-state inactivation is not known, but this region clearly contains domains important for modulation of inactivation properties of the $Ca_V2.2$ channel (12, 15, 25, 26). $Ca_V2.2$ isoforms lacking other segments of the II–III loop are more resistant to closed-state inactivation (25). The large variance associated with cumulative inactivation of $Ca_V2.2e[\Delta 18a]$ currents (Fig. 1*c*), although indirect, suggests the involvement of additional factors that have limited access. For example, syntaxin and SNAP-25 bind directly to the II–III loop of $Ca_V2.2e[\Delta 18a]$ and shift the voltage dependence of inactivation toward more hyperpolarized voltages (27–29). The synaptic protein-binding region encompasses exons 18 and 19 (30), and it will be interesting to determine whether exon 18a influences protein binding within this region.

Alternative splicing has the potential to generate a staggering number of structurally and functionally distinct classes of voltage-gated calcium channels from one $Ca_V\alpha_1$ gene (14). Exon 18a is present in rat, mouse, and human $Ca_V2.2$ genes, defined by consensus splice junction ag-gt, and expressed in rat, mouse, and human tissue (A. C. Gray and D.L., unpublished observations). A homologous exon is also present in the $Ca_V2.3$ gene. Its function is not known, but studies have linked it to Ca-sensitive regulation of the channel (18–20, 31). Exon 18a of $Ca_V2.2$ is expressed abundantly in caudal regions of the mammalian nervous system and in peripheral nerve ganglia (15). In sympathetic neurons and in the spinal cord of adult mammals, $Ca_V2.2e[+18a]$ mRNAs far exceed that of $Ca_V2.2e[\Delta 18a]$, suggesting that this splice isoform is present at presynaptic nerve terminals and regulates transmitter release in these regions of the nervous system. We demonstrate that exon 18a enhances the ability of $Ca_V2.2$ channels to sustain calcium entry during a train of action potentials. The dynamics of facilitation (32), augmentation (33), and potentiation (34) of synaptic transmission are linked to calcium concentration in the terminal (for review, see ref. 35). Our results predict that synapses that use $Ca_V2.2e[+18a]$ channels will support more sustained Ca entry during action potential trains than those that use $Ca_V2.2e[\Delta 18a]$.

We thank Dr. Yingxin Lin for providing $Ca_V\alpha_2\delta_1$ and Dr. Kevin P. Campbell for $Ca_V\beta_{1b}$. This work was supported by National Institutes of Health Grants NS29967 (to D.L.) and T32 MH19118 and NS43082 (to C.T.). A.C.G. is a Howard Hughes Medical Institute Predoctoral Fellow.

1. Dunlap, K., Luebke, J. I. & Turner, T. J. (1995) *Trends Neurosci.* **18,** 89–98.
2. Forsythe, I. D., Tsujimoto, T., Barnes-Davies, M., Cuttle, M. F. & Takahashi, T. (1998) *Neuron* **20,** 797–807.
3. Park, D. & Dunlap, K. (1998) *J. Neurosci.* **18,** 6757–6766.
4. McNaughton, N. C., Bleakman, D. & Randall, A. D. (1998) *Neuropharmacology* **37,** 67–81.
5. Jones, L. P., DeMaria, C. D. & Yue, D. T. (1999) *Biophys. J.* **76,** 2530–2552.
6. Patil, P. G., Brody, D. L. & Yue, D. T. (1998) *Neuron* **20,** 1027–1038.
7. Aldrich, R. W. (1981) *Biophys. J.* **36,** 519–532.
8. Toth, P. T. & Miller, R. J. (1995) *J. Physiol. (London)* **485,** 43–57.
9. Serrano, J. R., Perez-Reyes, E. & Jones, S. W. (1999) *J. Gen. Physiol.* **114,** 185–201.
10. Kozlov, A. S., McKenna, F., Lee, J. H., Cribbs, L. L., Perez-Reyes, E., Feltz, A. & Lambert, R. C. (1999) *Eur. J. Neurosci.* **11,** 4149–4158.
11. Chemin, J., Monteil, A., Bourinet, E., Nargeot, J. & Lory, P. (2001) *Biophys. J.* **80,** 1238–1250.
12. Degtiar, V. E., Scheller, R. H. & Tsien, R. W. (2000) *J. Neurosci.* **20,** 4355–4367.
13. Zhong, H., Yokoyama, C. T., Scheuer, T. & Catterall, W. A. (1999) *Nat. Neurosci.* **2,** 939–941.
14. Lipscombe, D., Pan, J. Q. & Gray, A. C. (2002) *Mol. Neurobiol.* **26,** 21–44.
15. Pan, J. Q. & Lipscombe, D. (2000) *J. Neurosci.* **20,** 4769–4775.
16. Ghasemzadeh, M. B., Pierce, R. C. & Kalivas, P. W. (1999) *J. Neurochem.* **73,** 1718–1723.
17. Williams, M. E., Marubio, L. M., Deal, C. R., Hans, M., Brust, P. F., Philipson, L. H., Miller, R. J., Johnson, E. C., Harpold, M. M. & Ellis, S. B. (1994) *J. Biol. Chem.* **269,** 22347–22357.
18. Pereverzev, A., Klockner, U., Henry, M., Grabsch, H., Vajna, R., Olyschlager, S., Viatchenko-Karpinski, S., Schroder, R., Hescheler, J. & Schneider, T. (1998) *Eur. J. Neurosci.* **10,** 916–925.
19. Pereverzev, A., Leroy, J., Krieger, A., Malecot, C. O., Hescheler, J., Pfitzer, G., Klockner, U. & Schneider, T. (2002) *Mol. Cell. Neurosci.* **21,** 352–365.
20. Leroy, J., Pereverzev, A., Vajna, R., Qin, N., Pfitzer, G., Hescheler, J., Malecot, C. O., Schneider, T. & Klockner, U. (2003) *Eur. J. Neurosci.* **18,** 841–855.
21. Lin, Z., Haus, S., Edgerton, J. & Lipscombe, D. (1997) *Neuron* **18,** 153–166.
22. Pragnell, M., Sakamoto, J., Jay, S. D. & Campbell, K. P. (1991) *FEBS Lett.* **291,** 253–258.
23. Coppola, T., Waldmann, R., Borsotto, M., Heurteaux, C., Romey, G., Mattei, M. G. & Lazdunski, M. (1994) *FEBS Lett.* **338,** 1–5.
24. Lipscombe, D. & Castiglioni, A. J. (2004) in *Calcium Channel Pharmacology*, ed. McDonough, S. I. (Kluwer, Boston), pp. 369–409.
25. Kaneko, S., Cooper, C. B., Nishioka, N., Yamasaki, H., Suzuki, A., Jarvis, S. E., Akaike, A., Satoh, M. & Zamponi, G. W. (2002) *J. Neurosci.* **22,** 82–92.
26. Bezprozvanny, I., Zhong, P., Scheller, R. H. & Tsien, R. W. (2000) *Proc. Natl. Acad. Sci. USA* **97,** 13943–13948.
27. Sheng, Z. H., Rettig, J., Takahashi, M. & Catterall, W. A. (1994) *Neuron* **13,** 1303–1313.
28. Sheng, Z. H., Rettig, J., Cook, T. & Catterall, W. A. (1996) *Nature* **379,** 451–454.
29. Bezprozvanny, I., Scheller, R. H. & Tsien, R. W. (1995) *Nature* **378,** 623–626.
30. Catterall, W. A. (1999) *Ann. N.Y. Acad. Sci.* **868,** 144–159.
31. Schramm, M., Vajna, R., Pereverzev, A., Tottene, A., Klockner, U., Pietrobon, D., Hescheler, J. & Schneider, T. (1999) *Neuroscience* **92,** 565–575.
32. Atluri, P. P. & Regehr, W. G. (1996) *J. Neurosci.* **16,** 5661–5671.
33. Brain, K. L. & Bennett, M. R. (1995) *J. Physiol. (London)* **489,** 637–648.
34. Delaney, K. R., Zucker, R. S. & Tank, D. W. (1989) *J. Neurosci.* **9,** 3558–3567.
35. Zucker, R. S. & Regehr, W. G. (2002) *Annu. Rev. Physiol.* **64,** 355–405.